Available online at www.sciencedirect.com
SCIENCE DIRECT
Materials Chemistry and Physics 96 (2006) 176–181
MATERIALS CHEMISTRY AND PHYSICS
www.elsevier.com/locate/matchemphys

Synthesis of thermally stable mesoporous titania nanoparticles via amine surfactant-mediated templating method

Hao Chen [a], Ke Dai [a,b], Tianyou Peng [b,*], Huanping Yang [b], De Zhao [b]

[a] *College of Science, Huazhong Agricultural University, Wuhan 430070, PR China*
[b] *Department of Chemistry, Wuhan University, Wuhan 430072, PR China*

Received 12 December 2004; received in revised form 23 June 2005; accepted 3 July 2005

Abstract

Mesoporous titania nanoparticles with high specific surface area and thermal stable anatase wall was synthesized from surfactant laurylamine hydrochloride (LAHC) and inorganic precursor $Ti(SO_4)_2$. The as-synthesized and calcined materials were characterized by X-ray diffraction, nitrogen adsorption–desorption, transmission electron micrographs, Fourier transform infrared spectroscopy and thermogravimetric analysis. The obtained mesoporous TiO_2 nanoparticles have mean diameter of 25.5 nm. The specific surface area of the mesoporous nanosized TiO_2 calcined at 400 °C exceeded 189 $m^2\,g^{-1}$, and that of the samples after calcinations at 500 °C still have 151 $m^2\,g^{-1}$. The obtained anatase mesoporous TiO_2 nanoparticles show relative high thermal stability.

Keywords: Laurylamine hydrochloride; Surfactant-mediated templating; Mesoporous titania; Nanoparticles

1. Introduction

Over the past decades, there has been increasing interest in the application of large surface area titania with nanoparticles and/or mesostructure for photocatalysts, photoelectrodes for solar energy conversion [1–20]. Among the three crystalline phases of anatase, rutile and brookite TiO_2, nanosized anatase TiO_2 is the most attractive for these applications because of its large effective surface area, which enhances the surface reactions. On the other hand, the smaller TiO_2 nanoparticles are also beneficial for the more effective photogenerated carriers separation and greater photocurrent, thus, the higher photocatalytic and photoelectrical chemical conversion efficiencies [1–3]. Therefore, there are numerous investigations on the synthesis of anatase phase with sizes ranging from 5 nm nanoparticles to several micrometers mesostructures and a variety of shapes for the photocatalysis and photoelectrode materials [4,5]. Generally, the precipitates derived from sol–gel process are amorphous [6], the photocatalytic and photoelectrical conversion efficiencies of those TiO_2 nanoparticles are not high enough for industrial purposes [7]. Hence, several methods have been reported to improve these situations, such as increasing the surface area, generation of defect structures to induce interfacial charge separation and modification of the TiO_2 with metal or other semiconductors [8,9].

Among those, mesoporous TiO_2 has attracted much attention due to its high surface-to-volume ratio and offers more active sites, which are of great importance in photocatalysis, photoelectrical chemical conversion [10]. Therefore, worldwide research activity based on mesoporous TiO_2 has ensued. However, it is quite difficult to synthesize TiO_2 with stable mesoporous structures because of their multitude of different coordination numbers and oxidation states [10–12]. The use of complex $Ti(OR)_{4-n}(AcAc)_n$ precursors, combined with phosphonate anionic surfactants in slightly acid medium, resulted in the first preparation of titania-based mesoporous oxide in 1995 [10]. However, they are not pure TiO_2 because a significant amount of phosphorous still remained in these materials and underwent partial collapse of the mesopores during template removal by calcinations. Thereafter, a tridentate ligand (triethanolamine) has been also used as stabilizer to product phosphorus-free

* Corresponding author. Tel.: +86 27 87218474; fax: +86 27 68754067.
E-mail address: typeng@whu.edu.cn (T. Peng).

0254-0584/$ – see front matter © 2005 Elsevier B.V. All rights reserved.
doi:10.1016/j.matchemphys.2005.07.003

wormlike, mesoporous TiO_2 [12]. Blanchard and co-workers have also used protons in acid media to retard the rapid condensation and generate titanium mesostructured oxosulfates or mesoporous oxophosphates [13,14]. Moreover, surfactants [15–17], triblock copolymer [18] and many non-surfactant organic compounds [19] have been successfully used to prepare mesoporous TiO_2. For example, laurylamine hydrochloride (LAHC) assemblies have also been applied as template yielded titania nanotubules and mesophase [17]. However, the obtained amorphous and semicrystalline TiO_2 have insignificant photocatalytic activity [20]. Calcinations at high temperature may not be beneficial for improving the photocatalytic activity, as the mesoporous framework has not been retained after heat treatment at 300 °C [21]. Since the anatase phase has a far higher photocatalytic and photoelectricalchemical conversion efficiency than amorphous and rutile TiO_2, it is still a challenge to synthesize mesoporous TiO_2 with high crystallization of anatase phase and large surface area [1,22,23].

We have fabricated titania microtubules with mesoporous walls as well as a large specific surface area in a LAHC/tetra-*n*-butyl-orthotitanate system. The obtained titania microtubules have a hierarchical organization of tubules-within-tubule with tubular nanochannels forming the walls of microtubules [11]. Herein, we apply a precipitation process to synthesize mesoporous anatase TiO_2 nanoparticles from laurylamine hydrochloride (LAHC) and $Ti(SO_4)_2$ in a facile and reproducible way. The obtained anatase porous TiO_2 nanoparticles show relative high thermal stability and surface area after heat treatment. To the best of our knowledge, there are few reports on the synthesis of TiO_2 nanoparticles with stable anatase mesoporous framework [22]. Those properties have some potential application in relate to photocatalytic and photoelectrochemical conversion, which is under progress in our group.

2. Experimental

All chemical reagents used in the experiments were obtained from commercial sources as guaranteed-graded reagents and used without further purification. We initially attempted to synthesize the mesostructure TiO_2 from LAHC and $Ti(SO_4)_2$, but this has found to result in TiO_2 nanoparticles. Further experiment improvement and characterization has been found that mesoporous structure in the obtained TiO_2 nanoparticles was formed.

In a typical process, 0.3918 g of $Ti(SO_4)_2$ was mixed with 0.2209 g of laurylamine hydrochloride (LAHC), then 4 ml of ethanol was added to the mixture under stirring. After 10 min, adding 4 ml of distilled water, stirring for another 2 h, the resulting mixtures was aged at ambient temperature for 48 h, and then at 100 °C in loosely closed vessel. After another 48 h, the mixtures were cooled to room temperature, and then the resulting powders were recovered by centrifugation, washed with water. After air-drying, the obtained solid was treated with ethanol for 1 h, and then centrifugation, washed with water and ethanol, then dried at 80 °C overnight. The as-prepared samples were calcined at different temperatures for 3 h to improve crystallinity with a heating rate of 2 °C min^{-1}, respectively.

Transmission electron microscopy images were obtained on a JEM-100X/II (TEM) and LaB6 JEM-2010(HT)-FEF (HRTEM) electron microscope. X-ray diffraction (XRD) patterns were obtained on XRD-6000 diffractometer using Cu Kα as radiation. The nitrogen adsorption–desorption isotherms at 77 K were measured on a Micrometrics ASAP 2010 system after samples were degassed at 120 °C. Fourier transform infrared spectra (FT-IR) on pellets of the samples mixed with KBr were recorded on a FT-IR-8201PC spectrometer. Thermogravimetric analysis (TGA) was conducted on the Netzsch STA449 simultaneous thermal analyzer.

3. Results and discussion

The as-synthesized sample shows broad anatase peaks (JCPDS, No. 21-1272, Fig. 1a), indicating the existence of nanocrystalline domain in the inorganic walls. It has been proved that the SO_4^{2-} anion and the acidic reaction condition (the initial pH in the present systems is ~0.6) can beneficial for the formation of anatase [24]. After heat treatment, only peaks of anatase phase that become stronger and sharper are identified in Fig. 1b–e. The intensity of peaks for anatase change slightly upon calcinations from 100 to 500 °C, indicating the anatase grains in the mesostructures have a relative high thermal stability. Even calcination at 900 °C for 3 h, the XRD pattern show that the main crystal phase is still anatase, and small peaks of rutile phase appeared (Fig. 1f). The crystalline phase transferred into rutile after calcinations of 1100 °C (Fig. 1g).

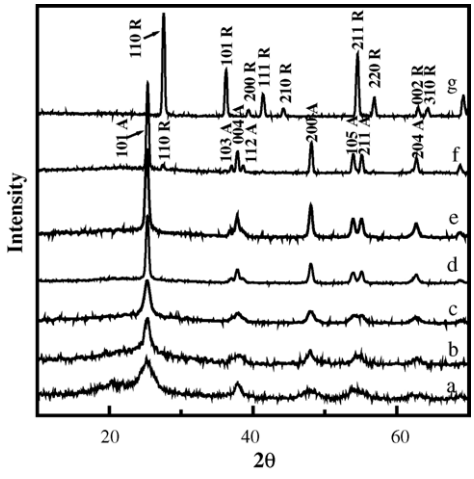

Fig. 1. High-angle XRD patterns of samples. (a) As-synthesized and calcined at (b) 300 °C, (c) 400 °C, (d) 500 °C, (e) 700 °C, (f) 900 °C, (g) 1100 °C.

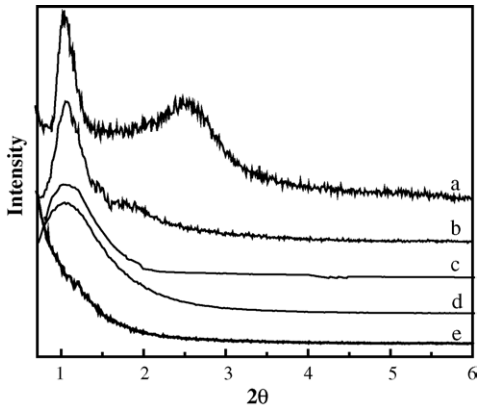

Fig. 2. Low-angle XRD patterns of samples. (a) As-synthesized and calcined at (b) 300 °C, (c) 400 °C, (d) 500 °C, (e) 700 °C.

The low-angle XRD patterns of the obtained samples are showed in Fig. 2a–e. For the samples as-synthesized and calcined at 300, 400 and 500 °C, all patterns are similar and exhibit a single diffraction peak corresponding to d-spacing of 9.45, 9.14, 9.02 and 8.90 nm, respectively. Although others have already demonstrated that similar single-reflection products still have short-range hexagonal symmetry [22], those single strong diffraction peaks of the calcined samples may just indicate the presence of mesostructure. The low-angle XRD patterns of the as-synthesized sample show two main broad peaks with shoulders at low angle regions, which cannot be ascribed to any ordered mesostructure. Upon calcinations from 300 to 500 °C, the peak broadening and the reduction in the intensity of the patterns is clearly due to the relatively wide range of pore diameter (ref. absorption data) of the calcined materials and the partial loss and/or collapse of the mesopores, as well as the nanosized property of our samples (ca. 25 nm, ref. below). No obvious peak is observed on low-angle XRD patterns for the sample calcined at 700 °C, suggesting the complete collapse of the mesoporous framework.

Fig. 3 shows the TEM micrographs of the samples calcined at different temperature. The nanoparticles as observation from TEM images (Fig. 3a–c) show porous characteristic. The more detail microstructure of the nanoparticles can be seen from the HRTEM images (Fig. 3b and c). The samples have relative uniform particles diameter in the range of 18–36 nm with mean particle size of 25.5 nm. Except for the samples calcined at 700 °C, porous structure without long-range order can be clearly observed in the obtained samples, which is coincides with the result of the low-angle XRD. The morphologies of pores and nanoparticles are changed insignificantly upon calcinations from 300 to 500 °C, indicating that reconstruction and/or collapse of the mesostructure are not occurred drastically. After calcinations at 700 °C, the powers ultimately change into nonporous nanoparticles with mean particle size of 24.6 nm (Fig. 2f). The inserted electron diffraction patterns in Fig. 3b and c indicated the polycrystalline properties in the mesoporous nanoparticles. Compared with sample calcined at 300 °C, the crystallinity of samples calcined at 400 °C was slightly enhanced as observation from the electron diffraction patterns. As can be seen form Fig. 3c and d, the pore size and the crystalline size of sample are estimated to be 1.8–6.0 and 2.5–4.5 nm, respectively. In previous work with PEO-based surfactants, Yang et al. found that these crystalline domains were embedded in the mostly amorphous TiO_2 matrix [18]. Cabrera et al. also reported the existences of 3 nm anatase in the mesoporous walls of wormlike materials [12]. In the present LAHC-templated TiO_2 system, however, the mesoporous wall basically composed of nanocrystal with limited amount of amorphous titania matrix, implying that the thermal treatment can efficiently crystallize the inorganic walls into anatase phase in the mesostrucutre. After calcinations at 700 °C, the anatase crystallites begin to grow extensively, then segregate from the mesostructures. Subsequently, the whole mesostructure is completely destroyed.

The TG–DTA curves (Fig. 4) of the as-synthesized sample revealed ca. 53% total weight loss on heating to 380 °C. The second exothermic peak began ca. 300 °C is attributed to combustion of organic compounds. Based on the mass loss, the products of the starting materials contain ca. 33% amine, indicating that the template cannot be displaced from the mesoporous framework by ethanol exchange. It means that in the present system, the self-assembly is $S^+X^-I^+$ mechanism [22,23], which will be further discussed below. DTA curve showed the LAHC begin to combust at about 300 °C, and the organic compounds can be removed completely after calcinations at 400 °C. The FT-IR spectra (Fig. 5) of the as-synthesized samples also indicate that the remained amine in the samples can be removed completely by calcinations at 400 °C. The IR-absorption band at 2920 and 2851 cm^{-1} (ν_{CH_3} and ν_{CH_2}) in the as-synthesized TiO_2 can be attributed to the characteristic frequencies of reminded LAHC. And there are no those peaks appeared in the FT-IR spectra of the sample calcined at 400 °C. It is believed that the broad peaks at 3400 and 1638 cm^{-1} correspond to the surface-adsorbed water and hydroxyl groups [16,23]. The decrease in the intensities of these peaks in the spectra of the samples with increased calcinations temperature confirms the diminishing the surface-adsorbed water and hydroxyl groups. The peaks at 460, 519, 620 and 910 cm^{-1} in the range of 400–1000 cm^{-1} are contribution from the anatase phase [16,23,25]. The intensities of this large band of the as-synthesized sample enhanced upon calcinations, implying the anatase phase has formed completely as the observation from XRD.

The as-synthesized sample show nonporous isotherm, which is reasonable considering that large amount of LAHC coexisted in the pores of as-synthesized sample as described in the FT-IR and thermal analysis. Due to the combustion of the organic compound, the samples after calcinations at 400 and 500 °C show an isotherms of type IV N_2 adsorption–desorption isotherms with hysteresis loops (Fig. 6), clearly indicating the mesoporous nature of TiO_2, but the considerable hysteresis loop at high relative pressures confirm that the mesopores were not too regular in

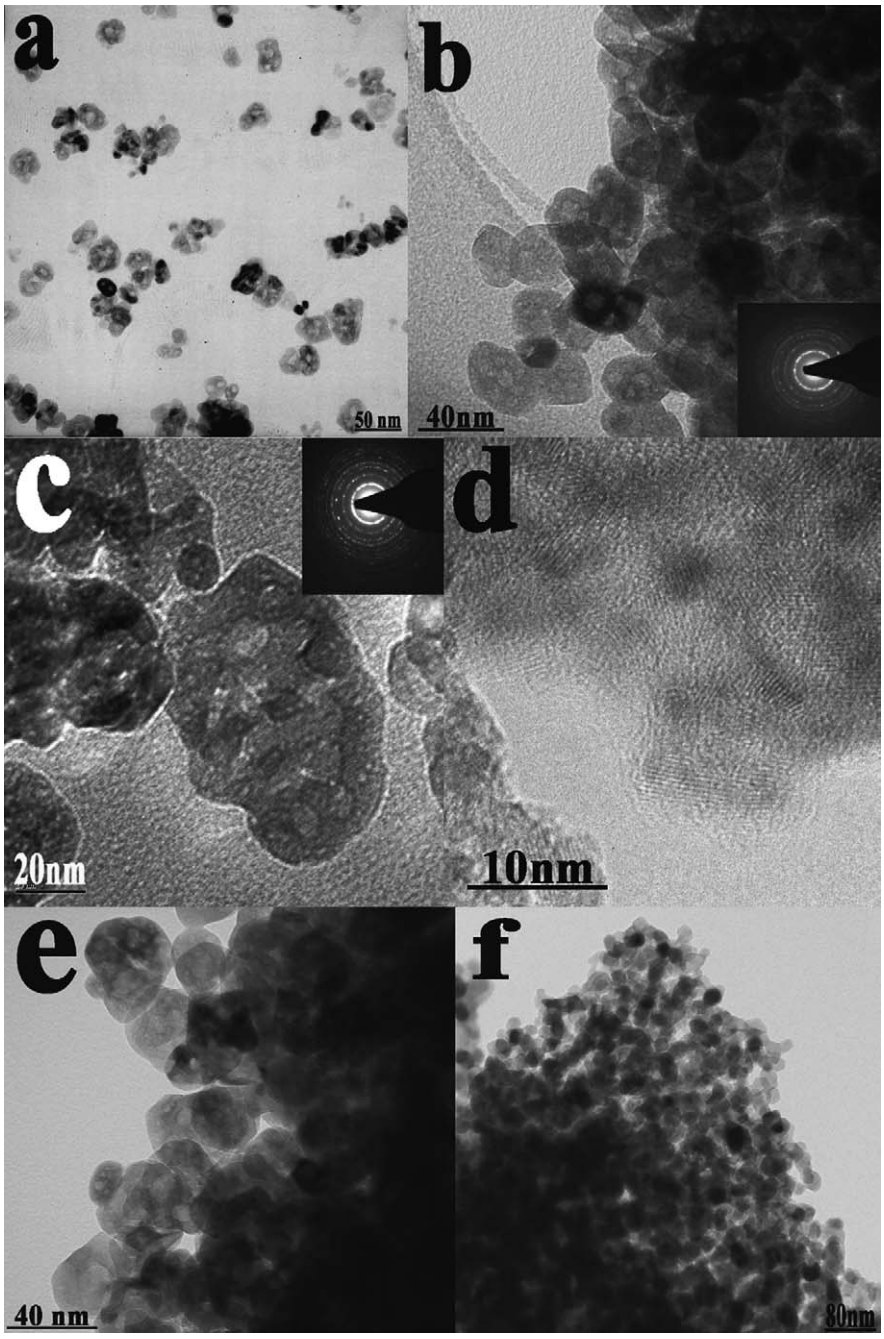

Fig. 3. TEM and HRTEM images of samples. (a and b) Calcined at 300 °C, (c) and (d) calcined at 400 °C, (e) calcined at 500 °C, (f) calcined at 700 °C.

the obtained samples. While considering that the mesopores and nanoparticles coexist in the obtained samples, it would be reasonable to think that the hysteresis loops can be attributed to the total contribution of both intra-particle pores and inter-particle pores. The pore size distribution determined from Barret–Joyner–Halenda (BJH) desorption isotherm for the sample calcined at 400 °C show a bimodal pore size distributions consist of smaller fine (2.0–5.5 nm) intra-particle pores and larger (8–20 nm) inter-particle pores (Fig. 6a). The 2.0–5.5 nm intra-particle pore size distribution centered 3.3 nm. The sample calcined at 500 °C still maintains relatively narrow intra-particle pore size distribution (2.0–7.5 nm) centered 3.7 nm (Fig. 6b). The pore increase in small degree can be attributed to the integrated results between the removals of the residual organic compounds in pores and the collapse together with shrinkage of mesoporous upon calcinations as described above. However, the pore size distribution of the inter-particle pores just changed slightly upon caclination, indicating that the inter-particles pores as well as the particle sizes changed insignificantly. The Brunauer–Emmett–Teller (BET) specific surface areas and pore volumes of samples are summarized in Table 1. For

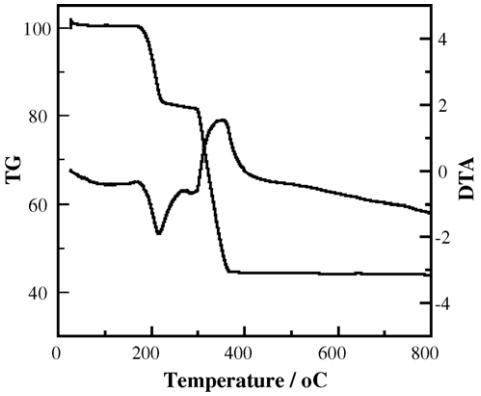

Fig. 4. TG–DTA curves of the as-synthesized sample.

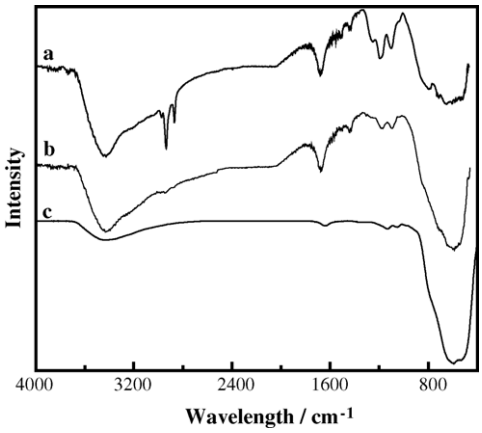

Fig. 5. FT-IR spectra of samples. (a) As-synthesized and calcined at (b) 300 °C and (c) 400 °C.

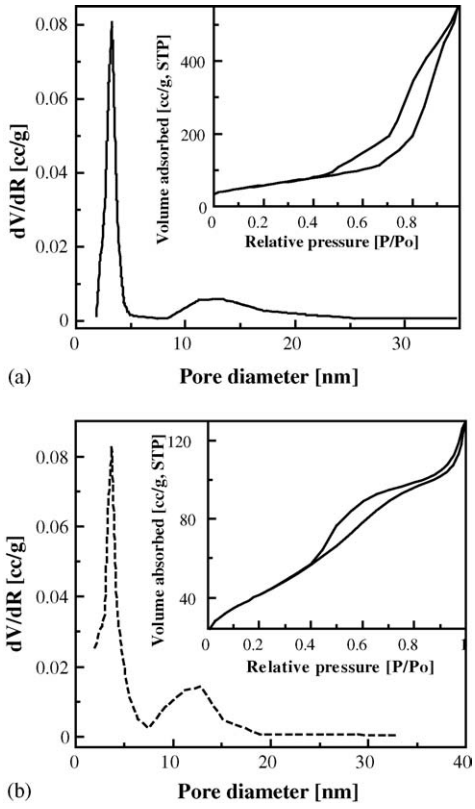

Fig. 6. N_2 adsorption–desorption isotherms (inset) and Barret–Joyner–Halenda (BJH) pore size distribution plots of samples calcined at (a) 400 °C and (b) 500 °C.

the sample calcined at 400 °C, the surface area is 189 $m^2\ g^{-1}$ with central pore diameter of 3.3 nm; the thickness of the pore wall (ca. 5.7 nm), estimated from XRD and porosity, significantly higher than that of the mesoporous MCM-41 silica materials. This fact probably favors the comparatively high thermal stability of the obtained materials. The relative high surface area (189 and 151 $m^2\ g^{-1}$) of sample calcined at 400 and 500 °C confirms that the framework of mesoporous TiO_2 is relative thermally stable. Moreover, the large reduction of surface area of the samples calcined at 700 °C show substantial pore damage or sintering, as indicated in Fig. 3f and Table 1. The surface areas and pore sizes of the obtained samples allow for comparison with previous work: Antonelli and Ying [10] (180 $m^2\ g^{-1}$, 3.2 nm calcined at 300 °C), Yang et al. [18] (205 $m^2\ g^{-1}$, 2.4 nm, calcined at 400 °C), Wang et al. [22] (246 $m^2\ g^{-1}$, 3.0 nm, calcined at 300 °C). The obtained materials present some useful characteristics for the photocatalysis and photoelectrical chemical conversion, such as the large and accessible pore surfaces, small crystal size and high crystallization of anatase mesoporous wall, etc.

Table 1
Summary of the physicochemical properties of mesoprous TiO_2 nanoparticles

Calcination temperatures (°C)	S_{BET}[a] ($m^2\ g^{-1}$)	Central pore size[b] (nm)	Total volume[c] ($cm^3\ g^{-1}$)
As-synthesized	8.3	–	0.04
300	212	3.3	0.23
400	189	3.4	0.20
500	151	3.7	0.21
700	51.5	–	0.19

[a] BET surface area calculated from the linear part of the BET plot.
[b] Estimated using the desorption branch of the isotherm.
[c] Single-point total pore volume of pores at $P/P_0 = 0.98$.

The ordered mesophase and/or mixed mesophase have been formed in many previous investigations along with the titania/CTAB and titania/LAHC literature [12–17]. The phase behavior of $TiOSO_4$/CTAB composite mesophase has been investigated [13,14]. It was shown that the initial step is a rapid formation (<300 ms) of either a pure lamellar, hexagonal or a mixed hexagonal/lamellar phase with a low degree of condensation, depending on the chain length of the surfactant as well as on the ionic strength of the solution. Due to the lower concentration of surfactant in the present system compared with the previous reports [13–17], it is impossible to form perfect ordered mesophase. Furthermore, the extended condensation is retarded by the lower pH condition. Therefore, only highly flexible organic–inorganic self-assemblies at a low degree of condensation maybe form in the initial stage. From this titanium-based hybrid self-assemblies,

the SO_4^{2-} ions would be expelled during the framework condensation while oxo or additional hydroxo bridges are formed between the titanium centers [13,14]. The SO_4^{2-} density and thus the charge density are therefore expected to decrease during the condensation of the inorganic framework. The removal of SO_4^{2-} during the condensation induces the expulsion of LAHC molecules from the pores in order to maintain the overall charge neutrality of the mesophase. Because $pH < pH_{iep}$ TiO_2, surface hydroxyl or $-OH_2^+$ groups are present [27]. Thus, the solid obtained from thermal treatment should present an $I^+X^-S^+$ type of interface ($X^- = Cl^-$). Therefore, we think a discrete hydrophilic nanosized Ti-oxo block are formed prior to the development of mesostructured hybrid phase in the present system [16,26–28]. As the further condensation of the inorganic framework, more and more surfactant will be expelled from the Ti-oxo block. Therefore, the relative concentration of the surfactant in the mixture will be gradually increasing, which may result in the formation of disordered liquid-crystal-like mesophases composed of preformed titania nanobuilding blocks, which are self-assembled around micelle assemblies within a liquid-crystal-like mesophase. At the same time, upon further condensation between Ti-oxo block, the directional growth of anatase phase inside the hybrid assembly maybe also occur at this stage. This mesophase is finally reinforced leading to robust inorganic mesostructure due to the condensation between inorganic compositions. On the other hand, due to the final products was present at pH <1 environment, as well as the lower concentration of surfactant, we can only obtain the nanoparticles with disordered mesophase. Thermal treatment of these products leads to high surface area TiO_2 nanoparticles with anatase phase wall in the mesoporous domains.

4. Conclusions

Mesoporous TiO_2 nanosized powders with high surface area and thermal stable anatase wall were prepared by using LAHC as templating agent via a precipitation processes. The obtained mesoporous TiO_2 nanoparticles have mean diameter of 25.5 nm with central pore size of 3.3 nm. The specific surface area of the mesoporous nanosized TiO_2 calcined at 400 °C exceeded 189 $m^2\,g^{-1}$, and that of the samples after calcination at 500 °C still have 151 $m^2\,g^{-1}$. The obtained anatase TiO_2 nanoparticles with mesostructures show relative high thermal stability. These mesoporous materials with anatase wall can be applied promisingly in photocatalysis and photoelectricalchemical application, which is under progress.

References

[1] J. Ovenstone, K. Yanagisawa, Chem. Mater. 11 (1999) 2770.
[2] Z. Zhang, C.C. Wang, R. Zakaria, J.Y. Ying, J. Phys. Chem. B 102 (1998) 10871.
[3] J.C. Yu, L.Z. Zhang, J.G. Yu, Chem. Mater. 14 (2002) 4647.
[4] Y. Murakami, T. Matsumoto, Y. Takasu, J. Phys. Chem. B 103 (1999) 1836.
[5] S. Komarneni, R.K. Rajha, H. Katsuki, Mater. Chem. Phys. 61 (1999) 503.
[6] C.C. Wang, J.Y. Ying, Chem. Mater. 11 (1999) 3113.
[7] Y.T. Kwon, K.Y. Song, W.I. Lee, G.J. Choi, Y.R. Do, J. Catal. 191 (2000) 192.
[8] C.N. Rusu, J.T. Yates, Langmuir 13 (1997) 4311.
[9] M.I. Litter, J.A. Navio, J. Photochem. Photobiol. A: Chem. 98 (1996) 171.
[10] D.M. Antonelli, Y.J. Ying, Angew. Chem. Int. Ed. Eng. 34 (1995) 2014.
[11] T.Y. Peng, A. Hasegawa, J.R. Qiu, K. Hirao, Chem. Mater. 15 (2003) 2011 (and therein references).
[12] S. Cabrera, J. El-Haskouri, A. Beltran-Portier, D. Beltran-Portier, M.D. Marcos, Solid State Sci. 2 (2000) 513.
[13] M. Linden, J. Blanchard, S. Schacht, S. Schunk, F. Schuth, Chem. Mater. 11 (1999) 3002.
[14] J. Blanchard, F. Schuth, P. Trens, M. Hudson, Microporous Mesoporous Mater. 39 (2000) 163.
[15] V.F. Stone Jr., R.J. Davis, Chem. Mater. 10 (1998) 1468.
[16] G.J.de A.A. Soler-IIIia, A. Louis, C. Sanchez, Chem. Mater. 14 (2002) 750.
[17] M. Adachi, Y. Murata, T. Harada, S. Yoshikawa, Chem. Lett. (2000) 942.
[18] P.D. Yang, D.Y. Zhao, D.I. Margolese, B.F. Chmelka, G.D. Stucky, Science 279 (1998) 548.
[19] C. Wang, Q. Li, R.D. Wang, Mater. Lett. 58 (2004) 1424;
J.Y. Zheng, J.B. Pang, K.Y. Qiu, Y. Wei, J. Mater. Chem. 11 (2001) 3367.
[20] B. Ohtani, Y. Ogawa, S.I. Nishimoto, J. Phys. Chem. B 101 (1997) 3746.
[21] S.H. Elder, Y. Gao, X. Li, J. Liu, D.E. McCready, C.F. Windisch, Chem. Mater. 10 (1998) 3140.
[22] Y.D. Wang, C.L. Ma, X.D. Sun, H.D. Li, Mater. Lett. 54 (2002) 359;
T.Y. Peng, D. Zhao, K. Dai, W. Shi, K. Hirao, J. Phys. Chem. B 109 (2005) 4947.
[23] J.C. Yu, L.Z. Zhang, Z. Zheng, J.C. Zhao, Chem. Mater. 15 (2003) 2280.
[24] M. Wu, G. Lin, D. Chen, G. Wang, D. He, S. Feng, R. Xu, Chem. Mater. 14 (2002) 1974.
[25] E.L. Crepaldi, G.J.de A.A. Soler-IIIia, D. Grosso, F. Cagnol, F. Ribot, J. Am. Chem. Soc. 125 (2003) 9770.
[26] Q. Huo, D.I. Margolese, U. Ciesla, D.G. Demuth, P. Feng, T.E. Gier, P. Sieger, A. Firouzi, B.F. Chmelka, F. Schuth, G.D. Stucky, Chem. Mater. 6 (1994) 1176.
[27] M. Kallala, C. Sanchez, B. Cabane, Phys. Rev. E 48 (1993) 3692.
[28] J. Blanchard, F. Ribot, C. Sanchez, P.V. Bellot, A. Trokiner, J. Non-Cryst. Solids 265 (2000) 83.